Quantum Electronics **31** (2) 159 – 163 (2001)

PACS numbers: 81.15.Fg; 79.20.Ds
DOI: 10.1070/QE2001v031n02ABEH001909

Probe-assisted study of the erosion plume upon the ablation of tantalum in vacuum by the 308-nm excimer laser radiation

O A Novodvorskii, E O Filippova, O D Khramova, A K Shevelev, C Wenzel, J W Bartha

***Abstract*. A Langmuir probe was used to study the erosion plume produced during the ablation of a tantalum target in vacuum by radiation from an excimer laser at 308 nm. The spatial and temporal dependences of the electron and ion currents of the probe were obtained in real time. The electron temperature of different regions of the plume at different distances from the target was measured for the first time from a series of dependences of the electron probe current on the probe voltage. The nonuniformity of the electron temperature and its lowering in different plume regions with increasing expansion time were determined. The ion density in the plume was determined at different distances from the target.**

***Keywords*:** *erosion plume, Langmuir probe, ion expansion velocity, electron temperature.*

1. Introduction

The laser ablation of solid targets has long been the subject of numerous studies. This is explained both by the complexity of the processes occurring during ablation and by the possibility of its wide practical applications [1, 2]. Among the important fields of employment of the solid-target ablation induced by laser radiation is the pulsed laser deposition of thin films.

For practical applications, especially upon laser-plasma deposition, the information on the characteristics of the erosion is needed. It is known that the ion energy spectrum plays an important role in thin-film deposition by physical methods [3], in particular, in the laser-plasma deposition [4]. Of prime significance in these processes is the possibility to control the ion energy spectrum, which has a pronounced effect on the characteristics of the films deposited (the type of the crystal structure, crystal dimensions, adhesion, etc.) [4]. The determination of the energy plume parameters (ion energy spectrum, electron temperature, density), their dependence on the energy of a laser pulse, the spatial evolution, and the angular dependence are of special interest when pulsed laser deposition is employed to produce thin metal films. Time- and space-resolved measurements during the plume motion from the target to the substrate provide the information on the kinetics of different particles and their propagation velocity.

Probe methods of research [5, 6 – 9] are widely used to study the laser erosion plume in the ablation of metals, semiconductors, ion crystals, and ceramics. The laser ablation of metals is characterised by the proximity of the thresholds of target vaporisation and plasma formation [10], and therefore the erosion plumes of metals are significantly ionised in pulsed laser deposition [5, 11]. In a strongly ionised plasma of the plume, an electric Langmuir probe detects charged particles, which constitute a substantial fraction of the plume particles, and in doing this provides a high locality of measurements.

Langmuir probes have been used to determine the ion velocity distribution [6, 9], the saturation potential of the ion current [9], the energy spectrum of copper ions [5], and the electron temperature of the erosion plume [7, 8]. In the ablation of MgO targets, the electron temperature was found to vary from 1 to 10 eV as the radiation energy density on the target was varied from 1.4 to 3 J cm^{-2} [3]. However, the studies of the electron temperature distribution over different plume regions and its time variation have not been conducted previously.

Here, a Langmuir probe was used to study the erosion plume in the ablation of a tantalum target exposed to the radiation of an excimer laser ($\lambda = 308$ nm). The spatial and temporal dependences of the electron and ion currents of the probe, the ion velocity distribution, the distributions of the electron temperature and the ion density in the plume, and also the dynamics of these parameters were studied in the real-time mode.

2. Experimental

Experiments were conducted in the VUP-5 vacuum chamber, which was evacuated with a diffusion pump to a pressure $p \leqslant 10^{-5}$ Torr. The erosion plasma was produced by the radiation of a XeCl excimer laser. The half-amplitude pulse duration was 20 ns and the pulse energy was varied from 2 to 25 mJ. The radiation was focused with a doublet objective with a focal distance of 8 cm and was directed to the target at an angle of 50° to the normal. The targets in the form of disks were made of a 99.9 %-pure tantalum foil with a thickness of 0.5 or 1 mm. The disks were attached to the motor shaft and rotated with a frequency up to 10 Hz.

O A Novodvorskii, E O Filippova, O D Khramova, A K Shevelev Institute of Laser and Information Technology Problems, Russian Academy of Sciences, ul. Svyatoozerskaya 1, 140700 Shatura, Moscow oblast, Russia
C Wenzel, J W Bartha Dresden University of Technology, Institute of Semiconductor and Microsystems Technology, D-01062 Dresden, Germany

Received 8 June 2000
Kvantovaya Elektronika **31** (2) 159 – 163 (2001)
Translated by E N Ragozin

The focal spot on the target was ellipsoidal in shape and had an area of 0.5 mm^2. The target and the walls of the vacuum chamber were grounded. The Langmuir probe 5 mm in length was made of a tungsten wire 0.2 mm in diameter placed in a ceramic tube. The probe voltage could be varied in the ± 18 V range. The source of adjustable probe voltage was an accumulator battery. One of its poles was connected to the probe via a potentiometer and the other was grounded via a load resistor. The source of adjustable voltage was shunted with a 2.5 μF capacitor to stabilise the probe voltage during the current pulse. The resistance of the load resistor was discretely variable from 10 to 1000 Ohm.

The signal from the load resistor was processed by a fast-response analogue-to-digital converter and stored in an IBM PC. The voltage range measured by the A to D converter was ± 5 V and the digitisation period was 0.1 μs long. The time of charge arrival at the probe was counted from the instant of the laser pulse generation recorded with a photodiode whose output was fed to the trigger input of the A to D converter. The probe was placed in the vacuum chamber (the probe axis was parallel to the target axis) and translated along the normal in the range from 3 to 160 mm from the target surface. The probe could be deflected out of the normal by $\pm 80^\circ$ to carry out the angular measurements.

To study the particles propagating along the target surface, the probe was moved at 3 mm above the target surface to a distance of up to 45 mm from the irradiation point. The probe axis remained parallel to the target surface in all the measurements; in this case the ablation region always viewed the side surface of the probe.

3. Experimental results and discussion

In the experiments conducted, we obtained over a thousand time-of-flight curves (TFCs) of the probe current for a tantalum ablation at different probe–target distances, for different energies of the incident laser radiation, and different probe voltages. By changing the sign of the probe voltage, we obtained the TFCs both for ions and electrons. For the characteristic points of the TFCs, we constructed the current–voltage probe characteristics whose electron branches were used to determine the electron temperature and the ion branch was employed to determine the voltage of ion current saturation.

The arrival times for the leading ion groups were measured for several probe – target distances. The arrival time was determined from the delay of the leading edge of a probe signal, which was measured at half amplitude, relative to the laser pulse. The arrival time of the leading edge exhibited a direct proportionality to the probe – target distance. The ion expansion velocity was determined from the probe curves as the ratio of the probe – target distance to the time delay of the corresponding current pulse relative to the onset of the laser pulse.

For the leading Ta ion group in the plume, the expansion velocity is independent of the distance to the target and is 1.9×10^4 m s^{-1}. The resultant velocity satisfies the dependence $v \sim M^{-1/2}$, where M is the atomic weight of the element; this dependence was observed by other authors for barium, yttrium, and copper ions [12] for a laser radiation intensity of 100 MW cm^{-2}. Here, the measurements were conducted under similar conditions.

The probe TFCs for tantalum ions observed for different probe – target distances were found to vary greatly. The evolution of Ta ion TFCs with distance is shown in Fig. 1 for an energy density of laser radiation at the target of 2 J cm^{-2}. Since the signal amplitude lowers as the probe–target distance increases, the TFCs in Fig. 1 were drawn not to scale for the sake of clarity; all the curves were recorded for the same probe voltage equal to -18 V.

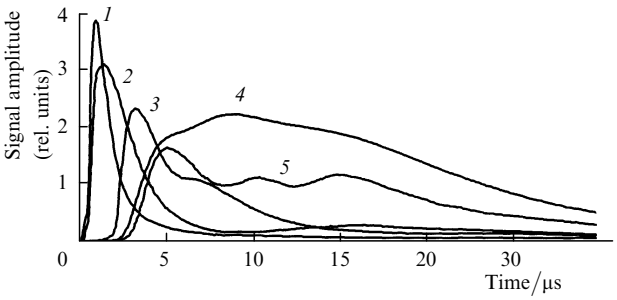

Figure 1. Probe TFCs for a probe potential of -18 V and probe – target separations $L = 10$ (*1*), 23 (*2*), 75 (*3*), 113 (*4*), and 133 mm (*5*). For clarity, the curves were scaled and the sweep time was reduced.

All the curves were recorded in the 0–100 time interval, but this interval is shortened to 30 μs in Fig. 1 to gain a better resolution. One can see from Fig. 1 that the delay of the leading edge of a signal is proportional to the probe–target distance.

When the probe–target distance is 10 mm (curve *1* in Fig. 1), the time-of-flight signal is a smooth curve with a single peak, a steep front, and a more gently sloping trailing edge which slopes down to zero in about 10 μs. If this curve is assumed to corresponds to some smooth ion velocity distribution, it should retain a smooth shape in the subsequent expansion. However, the time-of-flight signal was found to behave in a more complicated manner with increasing the probe – target distance. As the probe recedes from the target, there arise several peaks in the TFCs, which become more pronounced with distance. Referring to Fig. 1, the TFC has two peaks at distances of 23 and 75 mm. The third peak begins to manifest itself at a distance of 113 mm, and these three peaks come to be more clearly defined at 133 mm. It turned out that the velocity distribution in a group of particles that correspond to an individual peak in curves *4* and *5* can be described by the Maxwell distribution [13, 14]

$$I(t) = KLt^{-4} \exp\left[-\frac{(L/t)^2}{v^2}\right] \tag{1}$$

or the displaced Maxwell distribution [15]

$$I(t) = KLt^{-4} \exp\left[-\frac{(L/t - v_0)^2}{v^2}\right], \tag{2}$$

where K is the proportionality coefficient; $v = (2kT/M)^{1/2}$ is the most probable velocity; L is the probe – target distance; v_0 is the centre-of-mass velocity of the group of ions receding from the surface in the collisional mode. These distributions were taken to describe the resultant experimental data. Upon the mathematical treatment of the experimental data, it turned out that each of the curves *1*–*5*

in Fig. 1 is the sum of four Maxwell curves with different positions of the peaks. In other words, four groups of positively charged particles are observed in the plume for all the distances studied for a negative probe voltage.

As an illustration, Fig. 2 shows the TFCs for $L = 23$ and 113 mm averaged over ten experimental probe-current curves. Although two peaks are observable in the first curve and three peaks in the second one, both curves can be approximated by four Maxwell curves with a high degree of accuracy. For $L = 23$ mm, the TFC is approximated by the curves that peak at the points 1.1, 2.1, 4.0, and 16.7 μs, which correspond to particle velocities of 21, 11, 6, and 1.4 km s^{-1}.

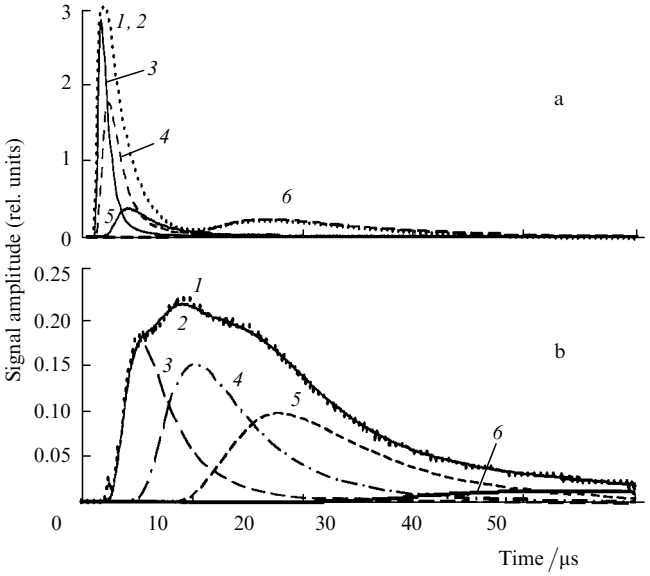

Figure 2. Approximation of the TFCs by Maxwell distributions for probe–target distances $L = 23$ (a) and 113 mm (b): (*1*) experimental curves obtained by averaging over ten single measurements; (*2*) their approximation by the sum of Maxwell curves *3*–*6*.

The curve obtained for $L = 113$ mm, which has three clearly defined peaks in its portion within 30 μs, is well approximated by three Maxwell curves. Approximating the portion of the curve for expansion times greater than 30 μs requires adding one more approximation – a displaced Maxwell distribution with a relatively low average velocity. These distributions peak at the points in time 5.3, 10.2, 17.7, and 49 μs to which there correspond the most probable velocities 21, 11, 6, and 2.5 km s^{-1}. One can see from the velocities obtained here for $L = 23$ and 113 mm that the velocities of the first three ion groups are constant whereas the velocity of the fourth group increases with distance to the target. The increase of the fourth group velocity is also confirmed by the TFC approximations for the remaining probe–target distances studied in our work (10 – 133 mm). Two- and three-modal ion velocity distributions were previously obtained by other authors for multicomponent targets of ion crystals [16] and HTSC ceramics [17].

Our earlier investigations revealed that the saturation of the ion current I_i in the ablation of Ta is reached for a probe voltage of ~ 10 V [18] and the current itself in the saturation regime is determined by the formula

$$I_i = 0.5SenV, \tag{3}$$

where S is the probe area; e is the electron charge; n is the ion density; V is the ion velocity at the boundary of the collisionless probe layer [19]. The ion time-of-flight signal is point-by-point convertible into a density distribution of the plume charges flying by:

$$n(t) = \frac{I(t)}{0.5SeV} = \frac{I(t)t}{0.5SeL}, \tag{4}$$

where t is the arrival time of the ions recorded. By taking advantage of these relationships, from the resultant TFCs we determined the particle density in the plume at different distances from the target. The peak ion density in the plume ranges from 3.3×10^{13} cm^{-3} at a distance $L = 10$ mm to 1.4×10^{11} cm^{-3} at a distance $L = 133$ mm.

The first ion groups traveling at a constant velocity are formed in the mode of free collisionless flow early in the ablation. The signal amplitudes for these groups fall off with distance as L^{-2} [18], which corresponds to the expansion of a spherical layer. Slower ion groups result from an outflow characterised by the occurrence of a Knudsen layer, when there originates a reverse particle flow to alter the conditions of subsequent vaporisation [14].

The evaporation of atoms from the target surface can take place for a time far greater than the laser pulse duration, as a result of the radiative heating of the target surface by the plume plasma and the reverse particle flow from the plasma. As follows from the hydrodynamic expansion model [20], the density of neutral particles retains a maximum at the target surface when the cloud expands to a distance of several centimetres. The neutral particles of the plume are known to disperse with lower velocities than the charged particles [12]. However, their leading fraction, which travels faster than the 'tails' of the fast ion groups, may be ionised owing to the resonance charge exchange to enhance the expansion velocity of slow ion groups. The long 'tail' in the probe TFCs may also form in the ionisation when the flow of neutral particles overlaps with the trailing edge of the electron cloud of the charged portion of the plume [8].

The cause for the origination of 'hot' electrons in the plume may be multiphoton absorption, bremsstrahlung [2], and the build-up of Langmuir oscillations [21]. Owing to the Coulomb interaction with the outer layers of the erosion plume, these electrons form the high-energy leading ion fraction where the ion energy can range into the hundreds of electronvolts, which is observed in the experiments [5, 18, 22]. However, owing to a low penetration depth of the external field in the plume plasma, the fraction of these ions is relatively low and amounts to several percent of the total number of ions [18, 22].

The time dependences of the electron probe current are, like the ion TFCs, complicated in shape. They vary greatly, depending on the probe–target distance. For long distances, several peaks are observed whose position in time is close to the peaks in the ion current TFCs. Fig. 3 gives a typical curve for the electron current of the probe, which was located for $L = 23$ mm in the plume axis. The dependence of the amplitudes of the TFC peaks on the probe voltage was used to determine the electron temperature T_e in the plume regions corresponding to these peaks.

The electron temperature was determined from the dependences of the logarithms of the peak amplitudes in the TFCs of the electron current on the probe voltage. The

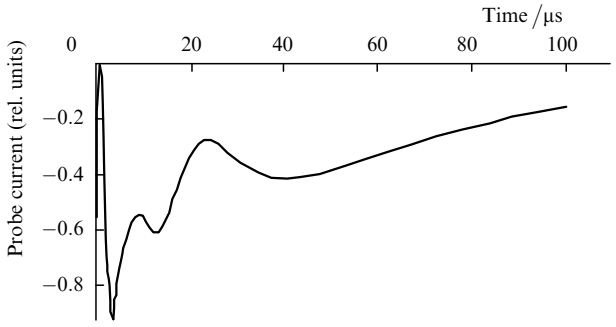

Figure 3. Pulse shape of the electron probe current at a distance of 23 mm along the target normal for a probe voltage of +8 V.

slopes of these dependences in the region below the saturation electron current are equal to $e/(kT_e)$. This follows from the probe equation

$$I_e \propto \exp\frac{eU}{kT_e},$$

where $U = U_s - U_p$ is the probe-to-plasma voltage; U_s is the probe potential; U_p is the plasma potential, which may differ from zero by kT_e/e; I_e is the probe current. The probe equation holds good for a positive probe voltage above kT_e/e, below which the ion current is commensurable with the electron one and the dependence $\ln I_e(U)$ deviates from linearity [19].

Table 1 gives the electron temperature T_e determined from the three observed peaks, whose position in time changes with the probe–target distance, for $L = 23$, 75, and 133 mm. The temperature proved to be different for all of the three peaks. We note the tendency for a temperature decrease towards the last peak, i.e., towards the tail of the plume. However, the resultant temperatures pertain to the electron clouds related to different ion groups which propagate with different velocities. If specific expansion velocities are, by analogy with the ion TFCs, ascribed to the peaks in the electron curves, the temporal positions of these peaks for different probe–target distances would permit us to distinguish the temperatures which correspond to the electron cloud related to a specific ion group and receding from the target with a constant velocity. Such are, for instance, the first three peaks for $L = 23$, 75, and 133 mm, to which there correspond electron temperatures of 6.4, 5.9, and 5.3 eV. Consequently, the electron temperature in the bunch, which moves with a constant velocity, falls off with distance to the target.

We estimate the electron temperature in the plume by the formula [23]

$$T_e = 2.98 \times 10^4 A^{1/8}(Z+1)^{-5/8} Z^{3/4} (I_{las}\lambda)^{1/2}\tau^{1/4} K,$$

Table 1. Electron temperature of the erosion plume (in electronvolts) for different probe–target distances L.

Peak in the TFC	L/mm		
	23	75	133
first	6.4	6.25	5.8
second	5.7	5.9	5.3
third	4.8	5.0	4.7

where A is the atomic weight of the ion; Z is the average ion charge in the cloud; I_{las} is the laser radiation intensity in W cm^{-2}; λ is the radiation wavelength in centimetres; τ is the laser pulse duration in seconds. For singly charged tantalum atoms ($Z = 1$) we obtain $T_e = 4.8$ eV; for $Z = 1.5$ (singly and doubly ionised tantalum atoms) $T_e = 5.6$ eV, which agrees well with the temperatures arrived at in our work. In the case of ion crystal ablation by an excimer laser, the authors of Ref. [16] also observed a lowering of the electron temperature T_e with distance to the target surface by measuring the electron temperature in the plume with the probe technique.

Early in the scan of the electron current probe curves, a short pulse is observed whose position in time is independent of the probe–target distance for a resolution of 0.1 μs. It is produced by the photoelectrons ejected from the target surface under laser irradiation prior to the onset of intensive ablation. A similar photoelectron pulse is observed in the ablation of dielectrics [8, 16]. The amplitude of these pulses also depends on the probe voltage. For them, the temperature measured at distances of 75 and 133 mm is $T_e = 11.5$ and 7.35 eV, respectively.

A study was made of the electron TFCs recorded in the translation of the probe along the target surface at 3 mm from the surface. In this case, the TFCs also exhibited three peaks. Fig. 4 gives a typical curve of the electron probe current, with the probe positioned near the target surface. One can see that the signal shape is significantly different from the shape of the current curve recorded when the probe was on the plume axis. The amplitude ratios of different peaks are also different. Also noteworthy is the absence of the photoelectron peak.

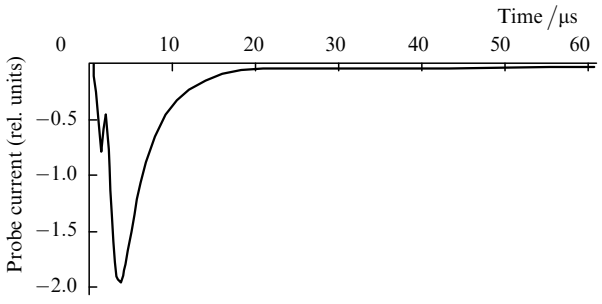

Figure 4. Electron-current pulse shape for a probe, located at 3 mm from the surface and offset by 30 mm from the plume axis, for a probe voltage of +8 V.

A separate peak is visible in the initial portion of the scan. This peak is weakly pronounced in or missing from the curves obtained when the probe was located on the target axis. This peak is produced by the electrons that disperse outside of ion cloud but are held by the coulomb forces. Owing to a large charge density in the cloud propagating along the normal, this peak is unresolved in the corresponding curves. In the direction parallel to the target surface, the charge density in the ion cloud is much lower (the ion expansion pattern is $\sim \cos\theta^6$ [18, 22]) and this peak is clearly defined.

The electron TFC peaks were used to measure the electron density. The dependences of the signal amplitudes on the probe voltage were measured for a probe–target-

normal distance of 15, 30, and 45 mm. The resultant T_e values appear in Table 2. The first and the second TFC peaks correspond to the ion groups propagating with constant velocities. It is seen that the temperature falls off with distance to the ablation region and also with approach to the tail of the plume. It should be noted that all the three temperatures in different regions of the plume located along the surface are lower than those along the normal to the surface.

Table 2. Electron temperature of the erosion plume (in electronvolts) for different distances between the probe and the target normal R.

Peak in the TFC	R/mm		
	15	30	45
first	4.2	3.9	2.90
second	4.0	3.65	1.85
third	3.3	2.6	1.80

4. Conclusions

The distribution of ion expansion velocity in the erosion plume in the ablation of tantalum in vacuum is uneven. The velocity distributions in individual ion groups are adequately described by a one-dimensional Maxwell distribution. The leading ion groups in the plume propagate with constant velocities. The slow ion groups accelerate during expansion. This may be caused by the ion density variation arising from recombination and chemical ionisation as well as by the change of ion expansion velocity arising from the collisions of the second kind. The accelerated ion motion in slow modes demonstrates the prevailing role of the electron and ion collisions with the neutral particles in the tail of the charged portion of the plume for the distances investigated. Here, the plasma does not yet reach the state of free expansion. The electron temperature of different regions of the plume at different distances from the target was measured from a series of the dependences of electron probe current on the probe voltage.

The electron temperature of the plume was found to be nonuniform, the temperature lowering from head to tail of the plume. Also observed is a temperature lowering with increasing expansion time throughout the plume.

References

1. *Hora H Physics of Laser-Driven Plasmas* (New York: Wiley, 1981; Moscow: Energoatomisdat, 1986)
2. Arutyunyan R V, Baranov V Yu, Bol'shov L A, et al. *Vozdeistvie Lazernogo Izlucheniya na Materialy* (Effect of Laser Radiation on Materials) (Moscow: Nauka, 1989)
3. Roy R A, Catania P, Saenger K L, Cuomo J J, Lossy R L *J. Vac. Sci. Technol., B* **11** 1921 (1993)
4. Saenger K L *J. Appl. Phys.* **70** 5629 (1991)
5. Jordan R, Cole D, Lunney J G, Mackay K, Givord D *Appl. Surf. Sci.* **86** 24 (1995)
6. Dyer P E, Greenough R D, Issa A, Key P H *Appl. Phys. Lett.* **53** 534 (1988)
7. Von Gutfeld R J, Dreyfus R W *Appl. Phys. Lett.* **54** 1212 (1989)
8. Ermer D R, Langford S C, Dickinson J T *J. Appl. Phys. B* **1** 1495 (1997)
9. Lubben D, Barnett S A, Suzuki K, Gorbatkin S, Greene J E *J. Vac. Sci. Technol. B* **3** 968 (1985)
10. Ready J F *Effects of High Power Laser Radiation* (New York: Academic Press, 1971)
11. Witke T, Ziegele H *Surf. Coat. Technol.* **97** 414 (1997)
12. Marine W, Gerri M, d'Anielo J M S *Appl. Surf. Sci.* **54** 264 (1992)
13. Anisimov S I *Zh. Eksp. Teor. Fiz.* **54** 339 (1968)
14. Kelly R, Dreyfus R W *Surf. Sci.* **198** 263 (1988)
15. Otis C E, Goodwin P M *J. Appl. Phys.* **73** 1957 (1993)
16. Chin J J, Ermer D R, Langford S C, Dickinson J T *Appl. Phys. A* **64** 7 (1997)
17. Boyarkin O V, Burimov V N, Golubev V S, Zherikhin A N, Popkov V L *Izv. Ross. Akad. Nauk Ser. Fiz.* **57** (12) 90 (1993)
18. Novodvorsky O A, Khramova O D, Shevelev A K, Filippova E O *Proc. SPIE Int. Soc. Opt. Eng.* **3885** 471 (1999)
19. Demidov V I, Kolobkov N V, Kudryavtsev A A *Zondovye Metody Issledovaniya Nizkotemperaturnoi Plazmy* (Probe Methods of Low-Temperature Plasma Research) (Moscow: Energoatomizdat, 1996)
20. Leboenf J N, Chen K R *Appl. Surf. Sci.* **96–98** 14 (1996)
21. Gorbunov L M, Kirsanov V I *Zh. Eksp. Teor. Fiz.* **96** 583 (1989) [*Sov. Phys. JETP* **69** (2) 329 (1989)]
22. Novodvorsky O A, Khramova O D, Filippova E O, Wenzel C, Bartha J W *Optics and Lasers in Eng.* **32** 449 (1999)
23. Phipps C R, Turner T P Jr, Harrison R F, et al. *J. Appl. Phys.* **64** 1083 (1988)